STScI | SPACE TELESCOPE SCIENCE INSTITUTE

Instrument Science Report STIS 2022-04(v1)

Recalibration of the STIS E140M Sensitivity Curve

Joleen Carlberg [1] , TalaWanda Monroe[1], Allyssa Riley[1], Svea Hernandez[1]

[1] Space Telescope Science Institute, Baltimore, MD

May 19, 2022

ABSTRACT

In 2012, the blaze function shapes (normalized sensitivity as a function of wavelength) of E140M's spectral orders began exhibiting changes that could not be accounted for with simple blaze shift coefficients in the PHOTTAB reference files. In February 2018, a special calibration program observed the HST standard star G191B2B in order to recharacterize the E140M blaze function shape and obtain a snapshot of the current sensitivity order-by-order. To best characterize the evolving shape changes across all post Servicing Mission 4 (post-SM4) data, 3 new PHOTTAB files and 2 new RIPTAB files were delivered in 2020. One pair of PHOTTAB and RIPTAB files correspond to the new blaze shape and associated blaze shift coefficients and are applied to data taken after July 01, 2016. The second RIPTAB file is associated with 2 PHOTTAB files that contain a rederivation of the original post-SM4 blaze shapes (covering data taken May 11, 2009 through July 01, 2016), with two different sets of blaze shift coefficients covering data taken before and after July 01, 2012. Two sets of blaze coefficients were needed to better calibrate the data where the shape was most actively evolving. As a side consequence of this work, spectral order 86 is newly flux calibrated for all post-SM4 data. These new sensitivity derivations benefited from the availability of new line blanketed model atmospheres of G191B2B that allowed a more robust identification of the stellar continuum in the observed data. These line blanketed models also predict continuum fluxes in the E140M bandpass that differ by a few percent relative to pure hydrogen models, and they became the new flux standard for the Hubble Space Telescope soon after the 2020 reference file delivery. Thus, all five reference files were redelivered in 2022 based on the new underlying flux model. While this ISR primarily describes the work and methods implemented for the 2020 new sensitivity curve derivations, it also describes both the blaze shift updates prior to 2018 that motivated the new observations, as well as the more recent update to the new CALSPEC v11 standard.

Contents

1. Introduction

The E140M grating onboard STIS has a single central wavelength at 1425 Å, offering broad FUV coverage at a resolving power of 45,800, and it is the most popular of STIS's four echelle gratings. After the cessation of the monthly offset positioning of echelle spectra in Aug. 2002 (see STIS IHB 7.6.2), E140M observations cover spectral orders 86-129 (44 orders) with a wavelength coverage of $\sim$1144–1730 Å. Prior to this date, the first and last spectral orders falling on the detector would vary with the monthly offset position. Consequently, not all spectral orders are equally well-calibrated, and spectral order 86 in particular has not been flux calibrated from 2012 onward, despite its routine presence on the detector.

Prior to the work described here, the most recent sensitivity calibration of STIS's echelle modes happened shortly after Servicing Mission 4 (post-SM4, May 2009 – present), as described in Bostroem et al. (2012). All of the echelle gratings are known to exhibit time and position dependent shifts in their blaze functions (the characteristic inter-order sensitivity function, also called the ripple function) due to the slight changes of angles of incidence (Aloisi 2006, Aloisi et al. 2007). When not corrected, these blaze shifts create characteristic residual slopes in the flux-calibrated data most easily identified by comparing the flux of consecutive spectral orders that have overlapping wavelengths. There is ongoing work to monitor the echelle data for these mismatches

and deliver updates to the blaze shift coefficients as needed (see STIS STANs for August 2017 and July 2018[1], and Table 1.)

In the course of updating the blaze shifts for E140M, Monroe (2018) found that shifting the blaze function could not sufficiently remove flux mismatches, as illustrated in Figure 1. Although new coefficients could remove the residual slopes, they introduced a new artifact—a sharp upturn in flux at the short-wavelength edges of the echelle orders that was suggestive of a change in the underlying shape of the blaze function. A special calibration program was proposed (PID 15381) to observe the primary standard star G191B2B to re-derive the blaze function and update the associated photometric throughput table (PHOTTAB) and ripple table (RIPTAB) for E140M. While the work to characterize the shape change for E140M was ongoing with these new data, the model atmospheres underlying the absolute flux calibration of all Hubble instruments were also undergoing revision (Bohlin et al. 2020), necessitating another delivery of references files to account for our improved understanding of the primary standard stars' spectral energy distributions.

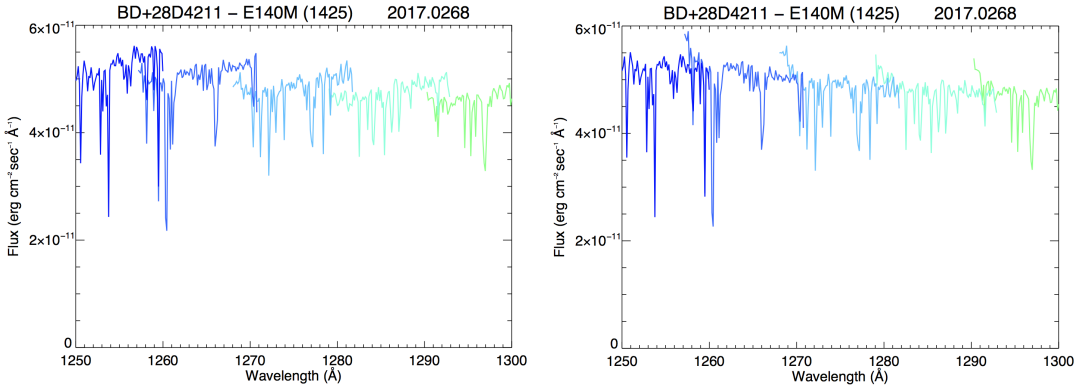

Figure 1. Spectrum of BD+28° 4211 with each spectral order plotted in a different color before (left panel) and after (right panel) the 2018 update of the blaze shift coefficients. The flux mismatches in overlapping wavelength regions of adjacent spectral orders in the left panel demonstrate the effects of an uncorrected blaze shift, However, with the best blaze shift coefficient corrections applied (right panel), artifacts at the order edges arise, suggesting that the underlying shape of the blaze function has changed.

1.1 Three Reference File Updates

The flux recalibration work described here refers to three separate reference file updates, which are included in Table 1. The first update was made to the FUV-MAMA

[1]At time of publication, these are available at `https://www.stsci.edu/contents/news/stis-stans/august-2017-stan.html` and `https://www.stsci.edu/contents/news/stis-stans/july-2018-stan.`

PHOTTAB on June 26, 2018, which contained characterization of the temporal E140M blaze function shift coefficients (`26p1601ko_pht.fits`). The calibration work described in Sections 2 – 6 of this report was carried out for the second set of reference file updates that were delivered on Aug. 07, 2020. These updates utilized the older CALSPEC standard model (version 07) to keep E140M calibrated on the same system as the rest of the STIS gratings (see Section 4). This delivery included three PHOTTAB and two RIPTAB reference files, with different `useafter` dates to better calibrate all post-SM4 data. Two of the PHOTTABs were based on PID 11866, for 2009 – 2012.5 (`48717027o_pht.fits`) and 2012.5 – 2016.5 (`48717026o_pht.fits`), to acommodate two different sets of blaze function shifts. The third PHOTTAB was based on PID 15381 and was applied after 2016.5 (`48717024o_pht.fits`). Only one RIPTAB update was needed for each PID, as shown in Table 1.

Efforts are underway to recalibrate all of the STIS modes to use the CALSPEC v11 models, which are described in detail in Bohlin et al. (2020). The procedures described in Sections 3 – 4 were repeated using the v11 models to produce new sets of sensitivity curves. The v11 models increased the FUV fluxes by $\sim$1% at 1150Å and $\lesssim$3% at 1700Å, as illustrated in Figure 2. Three new PHOTTAB reference files (two based on PID 11866 and one based on PID 15381) and two RIPTAB reference files were delivered to the pipeline on April 7, 2022, replacing the ones delivered in 2020. The PHOTTAB files have the same `useafter` dates as before: 2009 – 2012.5 (`6471930qo_pht.fits`), 2012.5 – 2016.5 (`64719317o_pht.fits`), and after 2016.5 (`6471930po_pht.fits`). The blaze shifts computed for the 2020 reference file updates were found to be sufficient for the 2022 updates, so these files only include updates to the sensitivity curves. All reference file updates are tabulated in Table 1.

2. Observations

2.1 Special Calibration Program: PID 15381

The primary HST flux standard star G191B2B was observed with three 703-sec exposures on Feb. 19, 2018. All three exposures (and their associated error and DQ arrays) are contained in a single dataset `odqw01010` in separate extensions. These exposures were taken during a time when the observatory jitter was often high and unpredictable. As reported in Osten (2018), Gyro-2 began showing noticeably larger jitter in the fall of 2017 and eventually failed in October 2018. In the interim, Gyro 1 unexpectedly failed on April 21, 2018. To ensure the observatory jitter did not impact the recorded flux, we inspected the RMS jitter along the V2 and V3 axes during the observations, as shown in Figure 3. The maximum peak-to-peak jitter amplitude along the noisier V3 axis was 61 mas. As the V2 and V3 axes are rotated at roughly 45° to the STIS slit, this corresponds to movement of $\sim$ 20% of the slit height and width in both the spatial and spectral dimensions. Despite these large excursions, for the majority of the observations the RMS is still quite small compared to the 0.2x0.2" slit (average RMS of 2.1 mas and 3.2 mas

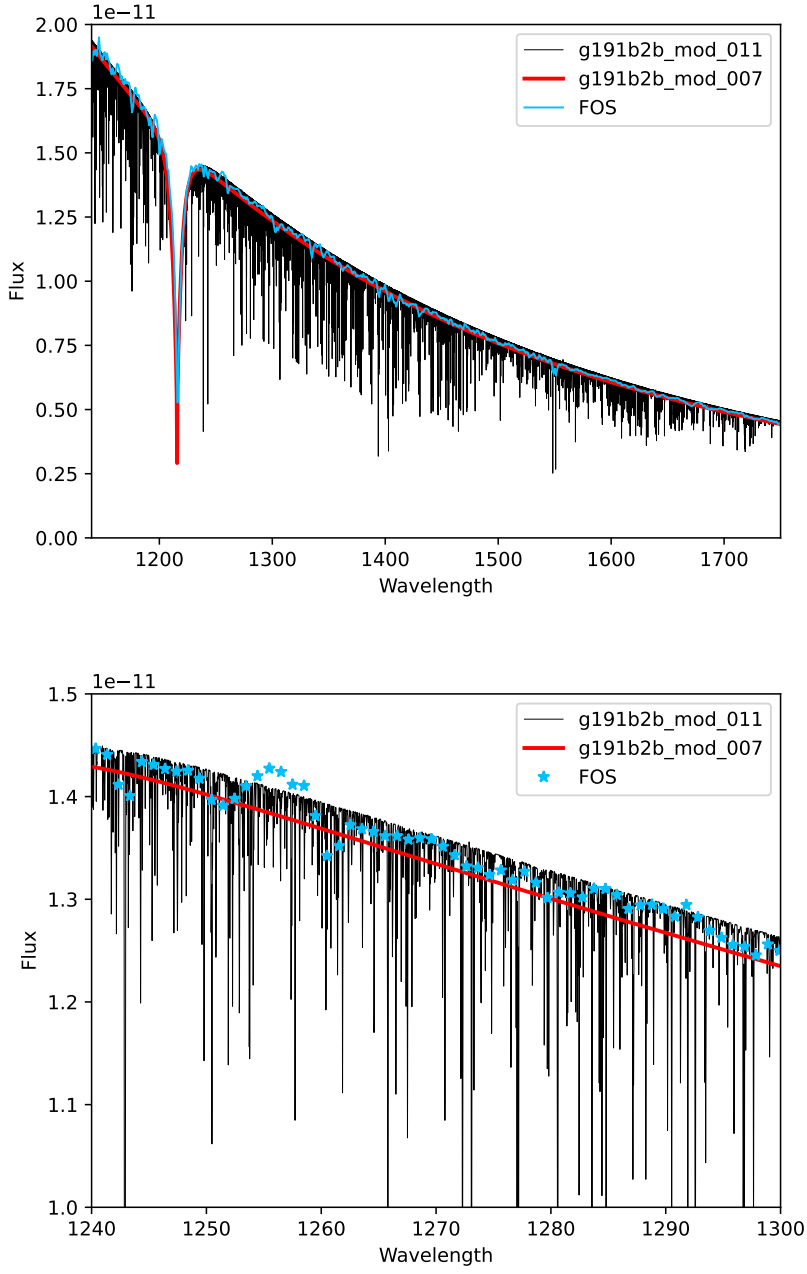

Figure 2. Comparison of the CALSPEC v07 hydrogen only models (red line) and v11 line-blanketed models (black line) of G191B2B. The observed FOS spectrum (blue stars) is also overplotted. The full wavelength coverage of E140M is shown on the top, and the bottom shows a portion of the spectrum just redward of the Lyman α line.

Table 1. E140M Reference File Updates

USEAFTER Date	PHOTTAB	RIPTAB	PID[a]	CALSPEC
2018 Blaze Shift Updates				
2009-05-11	26p1601ko_pht.fits	vb816446o_rip.fits[b]	11866	v07
2020 Sensitivity Curve and Blaze Shift Updates				
2009-05-11	48717027o_pht.fits	48717022o_rip.fits	11866	v07
2012-07-01	48717026o_pht.fits	48717022o_rip.fits	11866	v07
2016-07-01	48717024o_pht.fits	48717023o_rip.fits	15381	v07
2022 Sensitivity Curve Updates				
2009-05-11	6471930qo_pht.fits	6471931ao_rip.fits	11866	v11
2012-07-01	64719317o_pht.fits	6471931ao_rip.fits	11866	v11
2016-07-01	6471930po_pht.fits	6471930to_rip.fits	15381	v11

[a] Program ID used to derive the sensitivity curves. [b] This file was not updated in 2018, but included for reference.

along the V2 and V3 axes, respectively).

2.2 Archival: PID 11866

The sensitivity of E140M is also re-derived for early post-SM4 era observations using archival observations of G191B2B taken on Nov. 29, 2009, under program 11866. These three datasets `obb004070`, `obb0040a0`, and `obb0040b0` have exposure times of 695, 642, and 3200 s, respectively.

3. Overview of the E140M Recalibration Steps

Below is a high-level overview of the steps needed to create new PHOTTAB and RIPTAB tables for E140M. The PHOTTAB is created iteratively after the new RIPTAB is defined, because the RIPTAB affects the extracted net count rate as it factors into the scattered light model.

1. Divide NET count rate of observed spectra by the model to create inverse sensitivity functions (ISF)
2. Identify continuum regions in the ISFs and fit multi-nodal spline to continuum

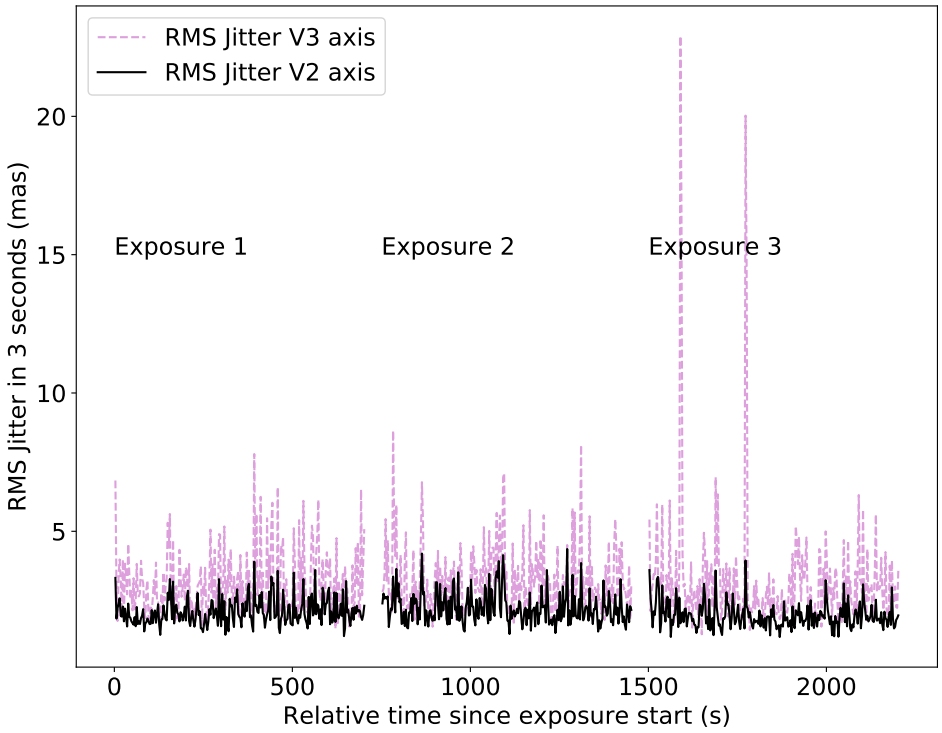

Figure 3. RMS jitter in mas during the observations of G191B2B. The bottom axis gives the time since the exposure start, and the second and third exposures have been offset horizontally by 750 sec and 1500 sec, respectively, for clarity. The solid black lines show the jitter along the V2 axis, while the dashed purple lines show jitter along the V3 axis.

3. Combine spline fits from individual ISFs and refit spline curves to the average ISF
4. Normalize the new spline curves to create the first iteration ripple function
5. Reprocess data using *calstis* and the new ripple function to extract updated NET counts, and repeat steps 1–4 to create a second ripple file
6. Remove time-dependent sensitivity from the average (unnormalized) ISF to create new throughput tables at a pre-defined early epoch
7. Recalibrate a suite of E140M data taken across the post-SM4 era with the new PHOTTAB and RIPTAB with no time-dependent blaze shift corrections
8. Rederive the time-dependent blaze shift coefficients (see Section 6)

4. Detailed Derivation of the Sensitivity Curves

4.1 The Use of Different CALSPEC Models

The 2020 updates for E140M used the TLUSTY atmosphere models of G191B2B as a calibrator to define the expected flux at a given wavelength (`g191b2b_mod_007.fits` in the CALSPEC v07 library). This pure hydrogen model only predicts the continuum emission of the white dwarf. However, the Rauch et al. (2013) line-blanketed NLTE model of G191B2B, which accounts for the metal line absorption, was also available in the CALSPEC v10 library (`g191b2b_mod_010.fits`). Like the v11 model used in 2022, the v10 model shows a redistribution of flux from the metal line absorption and slightly different continuum level compared with the hydrogen only model. Below $\sim$ 5500Å, the line-blanketed model predicts higher emergent flux, whereas lower fluxes are predicted at long wavelengths, as shown in Figure 2. To avoid introducing a systematic offset between the absolute flux calibration of the E140M grating with respect to G140L and G140M in 2020, those reference file updates continued to use the hydrogen-only atmosphere model to define the spectral energy distribution used to measure the ISF, while the line blanketed v10 model was used solely to mask regions of line absorption, as described in the next section. For the 2022 reference file update, the v11 line-blanketed model was used for both line masking and the underlying spectral energy distribution.

4.2 Fitting the Inverse Sensitivity Function

The ISF is defined in the observed reference frame, meaning that the wavelengths in the "x1d" files must have the velocity correction that placed the wavelength scale onto the heliocentric reference frame removed. Additionally, the model atmosphere wavelength scale, which is in the stellar rest frame, must be velocity shifted to account for both the known heliocentric radial velocity (22.0 km s^{-1}, Reid & Wegner, 1988) and the motion of the Earth. The model atmosphere is then resampled onto the wavelength scale of the observed data and divided into the net count rates to define the inverse sensitivity function.

Because the CALSPEC v07 model atmosphere used to define the ISF (for the 2020 update) does not include stellar absorption features other than the hydrogen Lyman series, strong lines must be masked out in the fitting. They are identified by taking the ratio of the Rauch et al. (2013, hereafter R13) line-blanketed model and the pure hydrogen model and then normalizing the continuum regions to remove the effects of line blanketing on the relative model continuum levels. Pixels that sit below a threshold of 0.97 are excluded from the ISF fitting as are the neighboring two pixels on either side of pixels below the threshold. Spectral order 104 contains the shadow of the repeller wire, and pixels 180–371 are also excluded from fitting in this order. The leading and trailing 8 pixels of each order are excluded to ensure the edges are well-behaved. Addi-

tional regions of the spectrum identified in wavelength bins are also masked out. They include:

1. Lyman α, 1214.35–1216.95 Å in the stellar rest frame
2. Lyman β, 1024.7–1026.7 Å in the stellar rest frame
3. Strong, unidentified stellar photospheric lines listed in Table 6 of R13 (± 0.05 Å)
4. Strong, ISM absorption features read off of Figure A.1 of R13 (± 0.05 Å)

Spline functions are fit to the ISF with Python's LSQUnivariateSpline in the *scipy* package. We use quadratic (k=2) splines, which are better behaved than higher order splines on spectral orders that have large regions excluded from the fit. After much experimentation with different node placement strategies, we decided to explicitly define the nodes to occur at pixel locations of 100, 200, 400, 650, and 800 pixels for all but two of spectral orders. For spectral order 121 (for which $\sim$2 Å of the blue edge are excluded because of the stellar Lyman α line) and spectral order 129 (for which the sensitivity is nearly zero below 1143 Å) we instead define 4 evenly spaced interior nodes, where the separation between the order edges and first (or last) node is the same as the interior node spacing. Figure 4 shows example fits to spectral orders 105 and 121.

The spline is fit to the non-masked portions of the ISF, and the resulting function is then evaluated onto the 500-element wavelength arrays in the then-current RIPTAB reference file (`vb816446o_rip.fits`). The resampled, interpolated ISFs from the three individual observations are averaged together without weights. This average ISF is refit with the same spline parameters and normalized to create the ripple functions for each spectral order.

The observations of G191B2B are then reprocessed with *calstis*, omitting the flux calibration and using the first iteration of the new ripple table created in the previous step. The ripple functions are used to create the scattered light model and the reprocessing results in slightly different net count rates. The new x1d files are then run through the same fitting procedure described above to create a second iteration of the ripple table, which is the one that will ultimately be delivered to CRDS.

4.3 Creating the PHOTTAB File

The unnormalized fits to the average ISFs from the second iteration then undergo further processing to create a new PHOTTAB. The time-dependent sensitivity coefficients in the TDSTAB `3ah1528co_tds.fits` are used to convert the sensitivities to the values they would have been at the reference time of MJD 50587.0 (1997.38 in decimal years). The TDS-corrected sensitivities are then converted to efficiencies following Equation 1 of Bostroem et al. (2012).

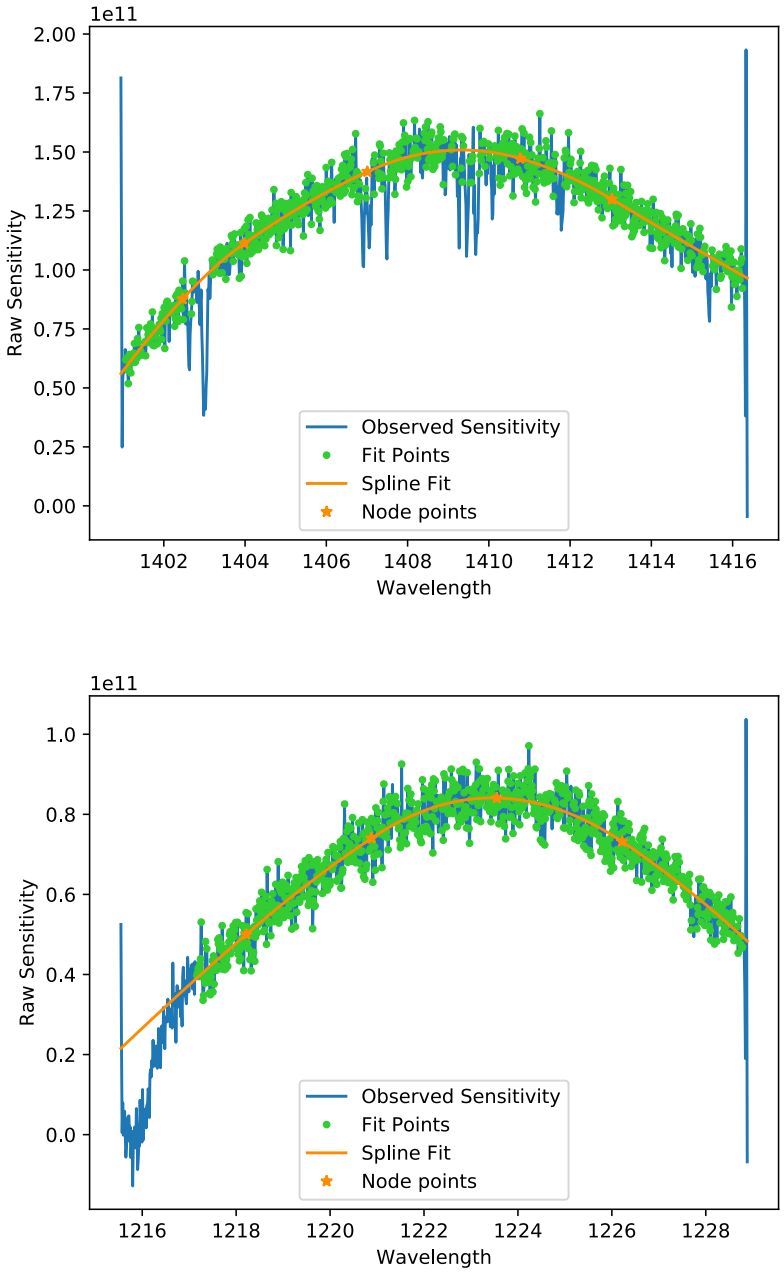

Figure 4. Example spline fits (orange lines) to the raw sensitivities of spectral orders 105 (top) and 121 (bottom) in the second science extension of dataset `odqw01010`. The full spectrum is plotted in blue, whereas the points retained for the spline fitting are shown as green points.

4.4 Special Considerations for Order 129

Spectral order 129 requires some special treatment because the sensitivity drops to nearly zero below ~ 1143 Å, and the spline fits tend to reach unphysical negative values. In the PHOTTAB file, wavelengths shorter than 1142.58 Å have the throughput set to zero so that *calstis* will not flux calibrate these values. However, the same strategy cannot be applied to the RIPTAB file. The ripple functions are only used by *calstis* in the calculation of the scattered light model, and the poorly defined regions at very low sensitivity can lead to spurious calculations of high amounts of scattered light at these short wavelengths that are not actually present. This in turn leads to over-subtraction of scattered light in neighboring orders. We found that more stable scattered light models are calculated if we adopt the ripple function (as a function of pixel) of neighboring order 128 for order 129. Such ripple function substitutions were also done by Bostroem et al. (2012), as indicated in their Table B.2.

4.5 Special Considerations for Order 86

Spectral order 86, covering a wavelength range of 1710–1730 Å, was not flux calibrated by Bostroem et al. (2012). However, its spectral trace is present in the current SPTRCTAB reference file; therefore, a non-flux calibrated spectrum (i.e., the NET count rate) can be trivially extracted by disabling the flux calibration correction step in *calstis*. Because spectral order 86 was newly added to the reference files in 2020, the wavelength arrays were generated as 500 evenly spaced points between 1710.76 Å and 1729.63 Å.

4.6 Rederivation of Post-SM4 Sensitivity

The above steps were repeated for observations of G191B2B taken on Nov. 29, 2009, under program 11866. Despite the disparate exposure times of the three datasets in question, unweighted averages were again used when combining the independently measured ISFs. A re-derivation of the early post-SM4 data was warranted to ensure that the sensitivities were derived in a consistent manner, and we found some improvements were made to some of the orders. In Figure 5, we show 5 different echelle orders of the standard star BD+28° 4211, which is regularly observed for the time dependent sensitivity monitor. This particular dataset was taken soon after STIS returned to operations, and should not yet have undergone any substantial change in sensitivity shape. By comparing to the FOS spectrum, it is clear that spectral orders 124–125 showed $> 3\%$ discrepancies with the original post-SM4 sensitivity derivation, while our sensitivity derivation for the 2020 update shows a much better agreement to the FOS spectrum.

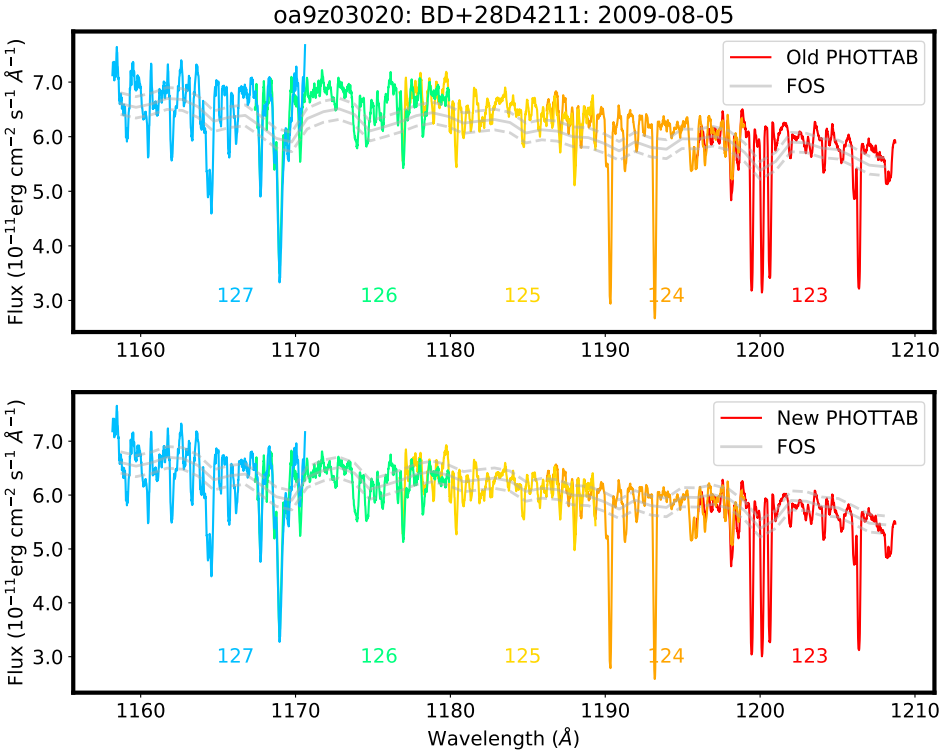

Figure 5. A dataset of the standard star BD+28° 4211 taken shortly after STIS returned to operations post-SM4. The different colors represent different echelle orders. The data has been box-car smoothed with a 15-point kernel. The gray solid line shows a reference FOS spectrum, and the dotted gray lines show $\pm 3\%$ deviations from the reference spectrum. The flux calibration for the top spectrum uses the original post-SM4 sensitivity derivations (Bostroem et al. 2012), while the calibration for bottom panel uses the newly derived sensitivities from the 11866 dataset for the 2020 updates.

5. Characterization of the Shape Change

In Figure 6 we show an order-by-order plot of the sensitivity function measured from both the immediate post-SM4 dataset and the data taken for the 2018 special calibration program. The temporal evolution of the shape is clear. The sensitivities of the shorter wavelengths in each order remain relatively constant, whereas the longer wavelengths show a relative increase in the sensitivity. This behavior causes the peak sensitivity of each order to shift to slightly longer wavelengths, which is why the temporal coefficients to the blaze shift equation were able to improve upon the flux calibration. However, since the shape change is more than just a mere shift, that correction introduced new errors in the flux calibration on the edges.

In Figure 7, we compare the *calstis* flux calibrated spectrum of BD+28° 4211 from dataset `odpce3020` calibrated with the previous RIPTAB and PHOTTAB files (2018 update) and the same spectrum calibrated with the newer versions of these reference files (2020 update). The improvement in the overall shape of the spectrum across the five spectral orders shown here is clear. There is also a systematic difference in the flux between these two calibrations. By comparing to the CALSPEC standard spectrum observed with the Faint Object Spectrograph (FOS), it is clear that using the 2020 reference files more accurately reproduces the absolute flux. The reason for the underestimate of the flux with the old reference files is that the blaze shift coefficients that were used to "flatten" the spectrum were optimized to get the longer wavelength edges of each order to better match the overall trend of the SED. However, as Figure 6 illustrates, it is the longer wavelength edges that have changed in sensitivity so that the previous blaze coefficients "pinned" the overall flux scale to the side of the blaze function that had changed in sensitivity.

6. Deriving New Blaze Coefficients

As mentioned in Section 1, both spatial and temporal changes to the angle of incident light on the E140M grating causes the blaze functions to shift with respect to the wavelength scale (Aloisi 2011; Boestrom et al. 2012), leading to flux discrepancies of 10% or more in the overlapping spectral regions of adjacent orders (e.g., Figure 1). Because all post-SM4 E140M observations are taken with a zero monthly offset, only the temporal component of the shift needs to be characterized for relative flux calibration in this era. Aloisi (2007, 2011) characterized the blaze function shifts for pre-SM4 data taken on the side 2 electronics with the following functional form:

$$BZS = BSHIFT\_VS\_X \cdot \Delta x + BSHIFT\_VS\_Y \cdot \Delta y + BSHIFT\_VS\_T \cdot \Delta t + BSHIFT\_OFFSET, \quad (1)$$

where BSHIFT_VS_X, BSHIFT_VS_Y, and BSHIFT_VS_T are linear coefficients for the

Figure 6. Comparison between the sensitivities of each echelle order as measured from the data taken as part of program 11866 and that taken as part of program 15381, using CALSPEC v07 models.

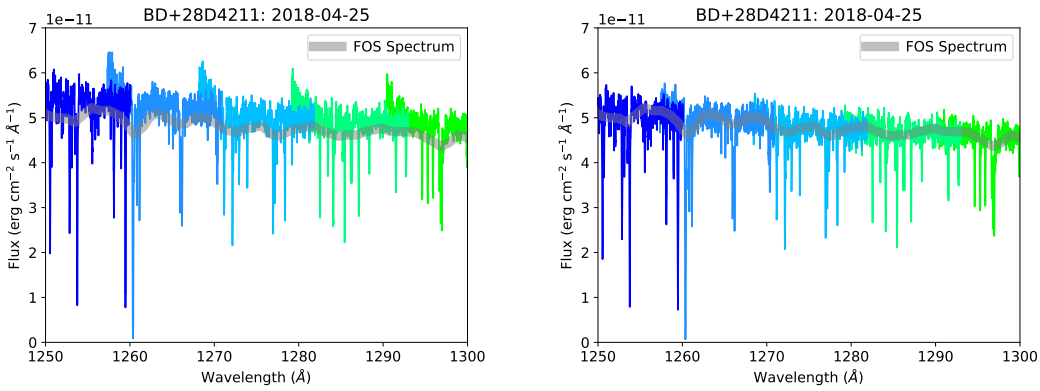

Figure 7. For a near contemporaneous TDS observation of BD+28° 4211, we compare the spectrum of BD+28° 4211 (spectral orders 114–119) flux calibrated with the 2018 pipeline reference files (left panel) to the same spectrum flux calibrated with the 2020 RIPTAB and PHOTTAB reference files (right panel). For reference, the FOS spectrum from the CALSPEC library is overplotted in gray.

dispersion direction (Δx), cross-dispersion direction (Δy), and observation time (Δt).[2] Aloisi (2007) started with the functional form parameterized by Bowers & Lindler (2003) for observations obtained with the side 1 electronics of the STIS instrument, but found that after the switch to side 2 electronics, the additional BSHIFT_OFFSET constant term was needed.

A 'modular' approach was taken by Aloisi et al. (2006, 2007, 2011) to determine the blaze function shifts for pre-SM4 data, whereby spatial and temporal changes in the blaze shift were corrected separately. The same approach has been implemented for post-SM4, but as mentioned above, the spatial components do not have a significant impact on the blaze shifts for this era, so the blaze shift coefficients from Bowers & Lindler (2003) were used for BSHIFT_VS_X and BSHIFT_VS_Y. Only the BSHIFT_VS_T and BSHIFT_OFFSET coefficients have been characterized for this work.

6.1 Blaze Function Shifts Calculations

This section outlines the more routine blaze shift coefficient calculations that were used both in the Monroe (2018) blaze coefficient update and in this work for the time period covering 2009–2012.5. In Section 6.2, we describe additional steps needed to derive the coefficients for data taken 2012.5 and onwards. A long temporal baseline for characterizing the blaze function shifts comes from observations of the spectrophotometric standard star BD+28° 4211 that have been routinely taken four times per HST cycle since SM4 (e.g., PIDs 11860, 12414, and 12775). The following procedure was followed:

[2]See Boestrom et al. (2012) for the formal definitions of these parameters.

1. A reference observation of BD+28° 4211, which is close in time to the G191B2B sensitivity curves observation, was identified to provide a temporal reference point for computing blaze shifts.

2. For each x1d file of BD+28° 4211, the NET count rates versus wavelength of each spectral order were fitted with a low order polynomial with sigma clipping rejection to mask absorption features and detector edge effects.

3. Each polynomial fit was normalized to its maximum value to crudely remove the impact of the time dependent sensitivity over time.

4. The total blaze function shift was computed for each spectral order of each observation with a cross correlation to the reference observation in step (1).

5. For each order and observation, the spatial component of the blaze shift was subtracted from the measured cross correlation shift. The average spatial blaze shift component was computed by *calstis* and is included in the header keyword BLZSHIFT (this step requires the time coefficients to be set to zero in the PHOTTAB).

6. Residual blaze shifts (after removing the spatial contributions) are examined versus Δt, the time difference between the observation date and the observation date of the sensitivity curves. A linear fit is carried out for each spectral order using all observations. The slope and y-intercept of the fits are the BSHIFT_VS_T and BSHIFT_OFFSET coefficients, respectively.

7. The ensemble of measured coefficients are then linearly fitted as a function of spectral order to reduce the noise within the fit of each order. The time and constant term coefficients are fitted separately, and the reference order in the PHOTTAB is used as a reference for these fits.

6.2 Impacts of the Shape Changes

The sensitivity curves derived from PID 11866 can well calibrate data taken between 2009 and 2012.5, when using appropriate blaze shift corrections derived as described in the previous section. Likewise, we found through testing that new temporal blaze function coefficients derived with reference to the epoch of the 15381 observations and using the 15381-derived sensitivity curves can well calibrate more recent data, taken 2016.5 through present day. However, the traditional method of deriving blaze function shift coefficients did not provide sufficient relative flux improvement in the overlapping regions of spectral orders for data taken between 2012.5 and 2016.5, due to the lack of a reference observation of G191B2B during that time. The polynomial fits of the NET count rates in step (3) above need to be similar in shape for the cross correlation procedure to produce robust blaze shift measurements, and this condition was likely not met during this timeframe.

A new method was used to derive blaze shifts for 2012.5 – 2016.5 observations with the Python package *stisblazefix* (Baer et al. 2018), available as a standalone post-processing tool.[3] The *stisblazefix* module assumes the blaze function alignment is a linear function of spectral order and then iterates to find the shift values that minimize the flux discrepancies of adjacent spectral orders. The *stisblazefix* package was executed on all observations of BD+28° 4211 and the resulting 'pixshift' array of shift values was saved and used in place of the cross correlations obtained in step (4) above. The 'pixshift' values for the reference observation were subtracted from each BD+28° 4211 observation, as well as the small spatial coefficient contributions, as in step (5), to compute the residual blaze shifts needed for the remaining steps (6) and (7) of the procedure listed above. In Figure 8, we compare the average temporal contributions of the blaze shifts of the new *stisblazefix* method compared to the traditional cross-correlation method with data calibrated with the 11866-derived sensitivity curves. Both methods give similar results from 2009 to roughly 2012.5, at which point the results from the two methods began to diverge with time by more than 5 pixels. This departure corresponds to when the blaze function shape changes began to emerge. The traditional cross correlation method relies more on the central peaks of the spectral orders, whereas the *stisblazefix* pixel shifts give priority to minimizing the flux discrepancies in the overlapping edges of adjacent orders. As discussed in Section 5, the peak sensitivity of the orders began to shift to slightly longer wavelengths and the longer wavelengths of each order also showed a relative increase in sensitivity, resulting in the two methods providing different measurements of the blaze shifts.

For data taken after 2012.5, we tested deriving temporal blaze shift coefficients from calibrations with both the older epoch and newer epoch sensitivity curves. We found that the calibration of the 2012.5 – 2016.5 observations using the PID 11866 set of sensitivity curves and blaze coefficients from the modified method provided a balance between the least amount of flux discrepancy in the overlapping regions of spectral orders, while minimizing other visual artifacts in the spectra. For observations taken after 2016.5, the new program 15381 sensitivity curves were used along with the modified procedures used for the 2012.5 – 2016.5 era to produce the best calibrated data products, after testing both methods. The program IDs used for the sensitivity curves, CALSPEC model atmosphere versions, and `useafter` dates for the pipeline reference files are included in Table 1 for all post-SM4 PHOTTAB and RIPTAB file updates.

6.3 Relative Flux Accuracy

The efficacy of the new sensitivity curves and blaze function coefficients were evaluated by comparing the relative flux agreement between overlapping wavelength regions of adjacent spectral orders, as shown in Figure 9 for observations of BD+28° 4211. The percent difference in the fluxes between the overlapping regions between the spectral orders was computed for each set of adjacent orders. The timespan of Figure 9 cov-

[3] https://stisblazefix.readthedocs.io/en/latest/

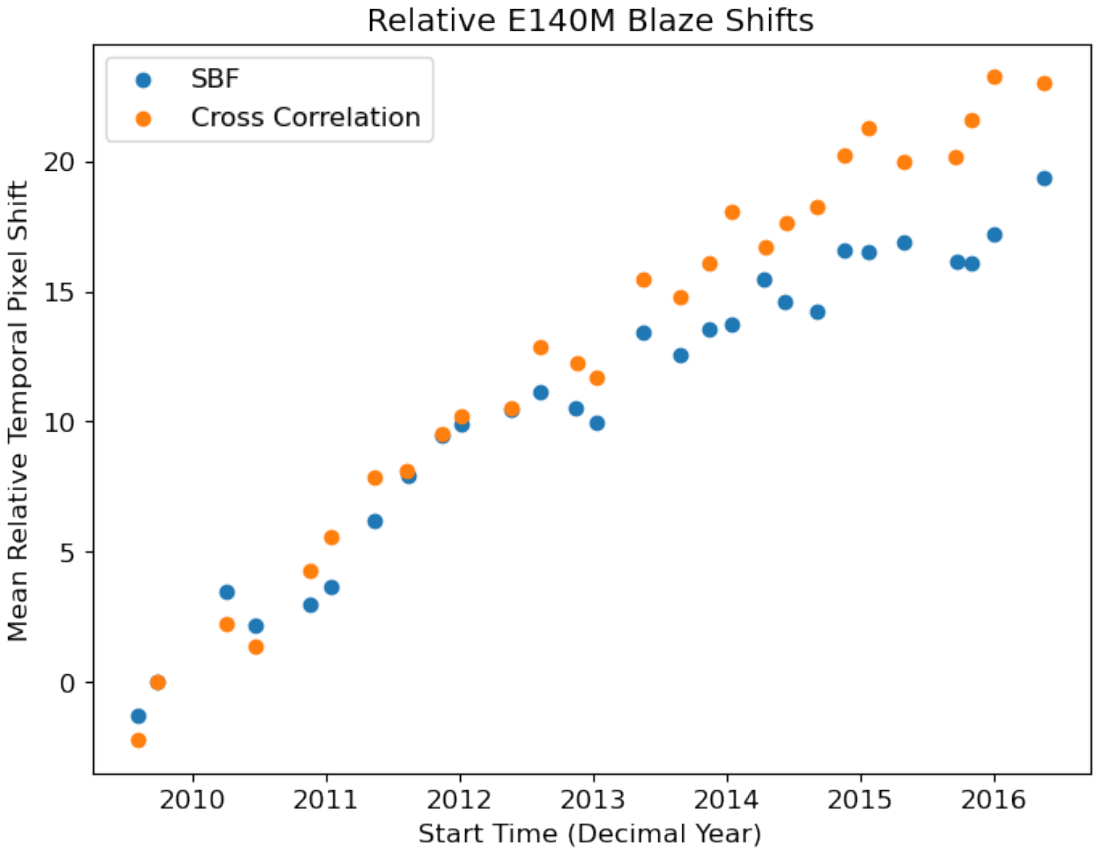

Figure 8. Temporal evolution of BD+28° 4211 E140M post-SM4 blaze function shifts. Two methods for measuring the E140M blaze function shifts are compared. Cross correlations relative to a reference data set are shown in orange. Shifts computed for observations calibrated with the new 2009 sensitivity curves from the *stisblazefix* (SBF) package are in blue. Both values have been adjusted to the same reference data set from 2009, and are averaged across all spectral orders. Note the diverging values between the two methods by mid-2012.

ers all of post-SM4, and the transitions between the three eras (2009 – 2012.5, 2012.5 – 2016.5, and 2016.5 – present) are marked with vertical lines. In this plot, the data corrected with the three new PHOTTAB files (blue data points) show clear jumps at these transition points. During the 2009 – 2012 era, our updated files had little impact on the percent differences and the spectra upon visual inspection, as the shapes of the sensitivity curves were previously well defined. The 2012.5 – 2016.5 time period was moderately impacted by the updated reference files by ∼1-2%, with the best improvements after 2014.5. Visual inspections of the calibrated spectra over these four years showed fewer artifacts, such as undulations in the flux of the spectral orders or the sharp upturns at the short wavelength edges of the orders (see Figure 10). Calibrations for the 2016.5 observations and later benefited the most with the new sensitivity curves derived

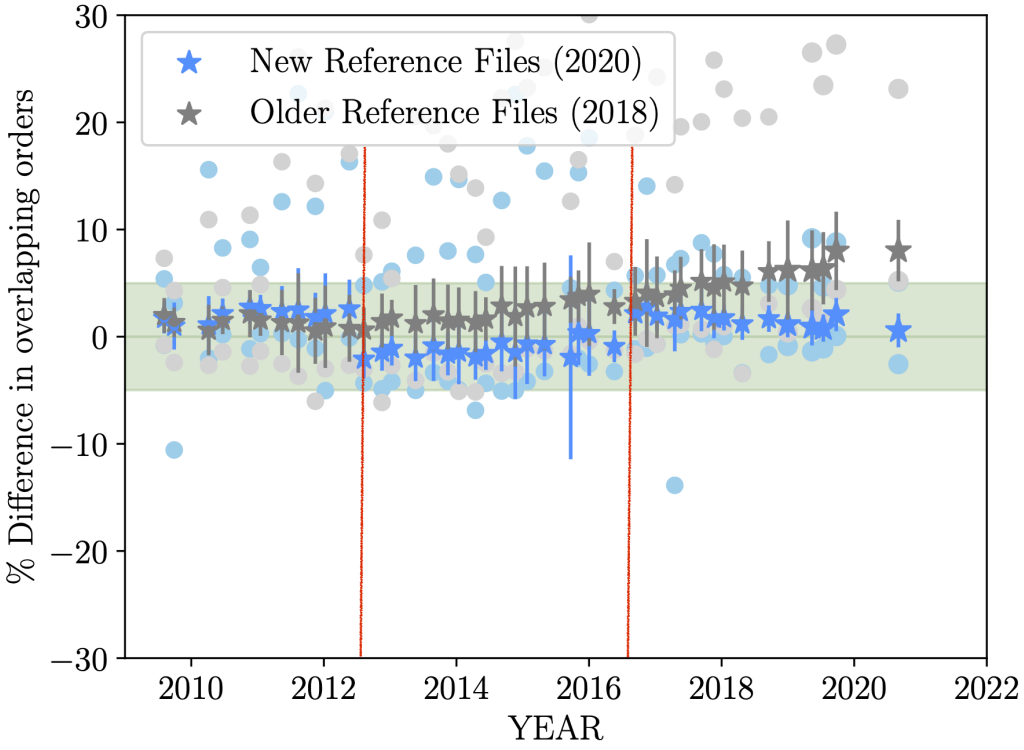

Figure 9. Relative flux agreement of BD+28° 4211 E140M post-SM4 observations. The average percent difference in flux between overlapping wavelength regions of all spectral orders is represented by the stars, along with the standard deviation of the mean as the error bars. The filled circles indicate the minimum and maximum percent differences between orders, for each observation. We have compared reductions using the older set of sensitivity curves derived from the 11866 observations in grey (`26p1601ko_pht.fits`) to the reductions using the three new PHOTTAB files delivered in 2020, in blue, as described in Section 6.3. The shaded green regions indicate $\pm$ 5% difference levels. The three eras spanned by the new reference files are delineated with red vertical lines.

from PID 15381 and the new blaze shift coefficients, with improvements as much as 3% in relative flux agreement for some observations in 2016 to improvements of over 5% at the latest epochs.

Figure 10 compares representative spectra from each of the three time eras using the old reference file from 2018 to the newer files delivered in 2020. The absolute flux calibration for E140M observations with the 0.2x0.2 aperture is guaranteed to be 8%, with a relative photometric accuracy of 5% within a given exposure (STIS IHB, Section 16.1). When Bostroem et al. (2012) used new post-SM4 G191B2B observations to derive sensitivity curves for post-SM4, the absolute flux calibration accuracy was

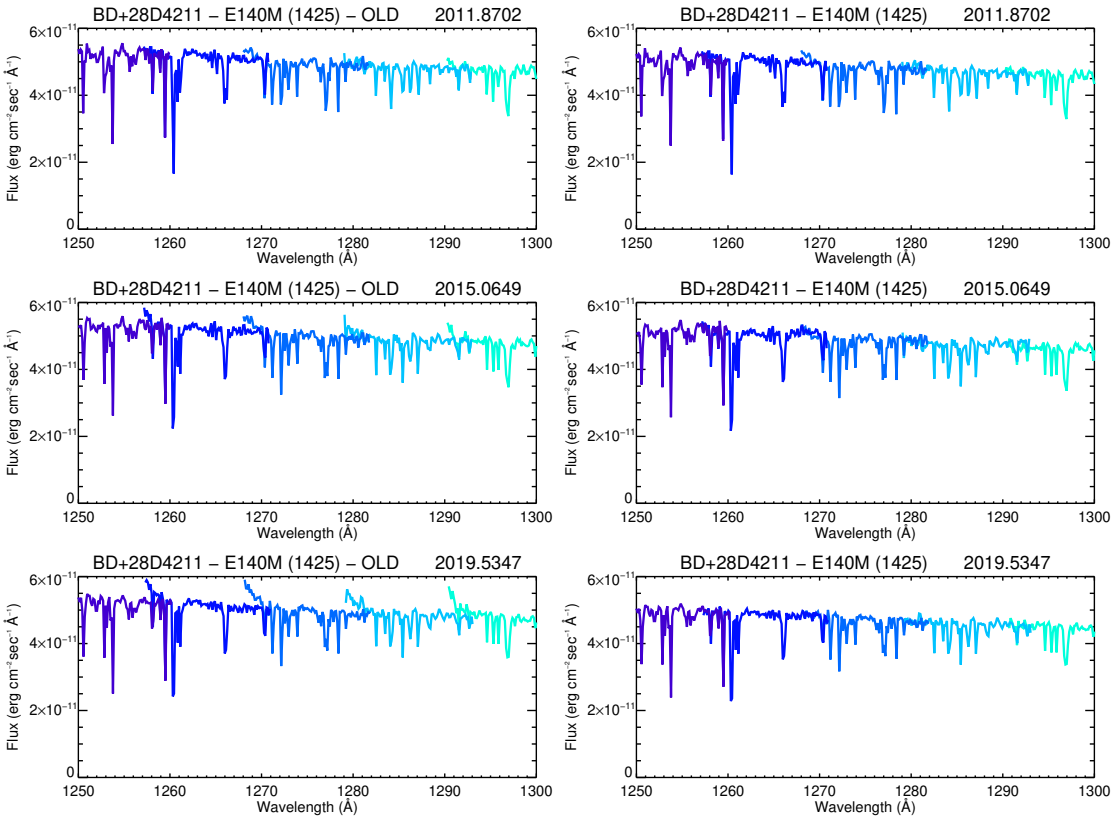

Figure 10. Example calibrations of BD+28° 4211 observations demonstrating the effectiveness of the new sensitivity curves and blaze function shifts from this work to improve both relative and absolute flux calibration for all post-SM4 E140M observations. Plots in the left column are using older sensitivity curves and blaze coefficients from the 2018 PHOTTAB update. Plots on the right use the updated sensitivity curves and blaze coefficients from the 2020 reference file updates.

improved to 5% for observations within a few years of SM4. Their error budget included an RMS scatter about the CALSPEC v07 model and intrinsic systematic uncertainty of the model itself. The relative flux uncertainties in our current work likely contribute up to 2-3% on average to the absolute calibration errors. Users requiring the most stringent flux accuracy possible for their observations are encouraged to use the *stisblazefix* tool, to possibly further optimize the blaze function shifts for their individual observations.

7. Summary

We have presented work done to improve the photometric calibration of E140M observations in the post-SM4 era through updates to blaze shift coefficients (in 2018 and 2020) and new or improved sensitivity curves (2020 and 2022). The focus of this ISR has been on the methodology for measuring order-by-order sensitivity curves and corresponding ripple functions to characterize the shape changes in these curves, as well as the derivation of sets of blaze shift coefficients to cover the period of time where the shapes were changing most rapidly (the 2020 reference file delivery). However, this new methodology is now being used for other STIS echelle modes as part of the much larger on-going initiative to bring all modes onto the CALSPEC v11 calibration system. The change from the CALSPEC v07 to v11 models has the largest impact in the FUV, where the model fluxes differ by up to 3%. A forthcoming report will summarize and detail the work for the recalibration effort to update all STIS modes to the CALSPEC v11 models. At the time of writing, only the following high priority modes are calibrated with v11 models: FUV/G140L, NUV/G230L, CCD/G230LB, CCD/G430L, and FUV/E140M (STIS STAN April 2022[4]).

Acknowledgements

We gratefully acknowledge Ralph Bohlin and Azalee Bostroem for valuable discussions about how past calibrations were conducted and to Azalee for providing us with extensive notes associated with the previous echelle sensitivity calibrations.

Change History for STIS ISR 2022-04

Version 1: May 19, 2022- Original Document

References

Aloisi, A. 2006, The 2005 HST Calibration Workshop: Hubble After the Transition to Two-Gyro Mode, 190

[4]At the time of this publication, available at `https://www.stsci.edu/contents/news/stis-stans/april-2022-stan.html`.

Aloisi, A., Bohlin, R., & Kim Quijano, J. 2007, STIS Instrument Science Report 2007-01
Aloisi, A. 2011, STIS Instrument Science Report 2011-04
Bohlin, R., Gordon, K. D., & Temblay, P.-E. 2014, PASP, 126, 711
Bohlin, R., Hubeny, I., & Rauch, T. 2020, AJ, 160, 21
Bostroem, K. A., Aloisi, A., Bohlin, R., Hodge, P., & Proffitt, C. 2012, STIS Instrument Science Report 2012-01
Bowers, C., & Lindler, D. 2003, 2002 HST Calibration Workshop, eds. S. Arribas, A. Koekemoer, & B. Whitmore (Baltimore: STScI), 127
Monroe, T., 2018, "More Accurate E140M Blaze Function Shifts in FUV PHOTTAB Delivery" , STIS STAN July 2018
Prichard, L., Welty, D. and Jones, A., et al. 2022 "STIS Instrument Handbook (IHB)," Version 21.0, (Baltimore: STScI)
Rauch, T., Werner, K., Bohlin, R., & Kruk, J. W. 2013, A&A, 560, A106
Reid, N. & Wegner, G. 1988, ApJ, 335,953